Crystal Growth

DOI: 10.1002/anie.201204747

Understanding the Formation and Evolution of Ceria Nanoparticles Under Hydrothermal Conditions**

*Christoffer Tyrsted, Kirsten Marie Ørnsbjerg Jensen, Espen Drath Bøjesen, Nina Lock, Mogens Christensen, Simon J. L. Billinge, and Bo Brummerstedt Iversen**

Cerium(IV) dioxide (ceria) based materials are attractive in many technological fields owing to their important properties such as ion conduction, reversible oxygen storage, and catalytic activity.[1] Ceria-based nanomaterials can be produced through different synthesis routes including pH-controlled precipitation, microemulsion, mechanochemical processing, and pyrolysis.[2a,b,c,d] In this context, hydrothermal and supercritical syntheses have attracted increasing attention as environmental friendly, readily adjustable one-step routes to the production of a wide variety of crystalline nanomaterials.[3] Nanomaterial properties often depend on their size regime,[4] requiring a detailed knowledge of the many diverse chemical processes and material changes taking place during the synthesis, when the soluble precursor complexes react and grow into stable nanoparticles of the product. However, the extreme conditions of elevated temperatures and pressure needed for hydrothermal/supercritical synthesis necessitate the use of thick-walled reaction chambers, making it difficult to study the chemical processes as they occur (in situ). This can be circumvented by highly penetrating probes such as high-energy X-rays. Here, we present an in situ study on the hydrothermal and supercritical synthesis of CeO_2 nanoparticles using a unique experimental setup that allows direct probing of the reaction mixture with synchrotron X-rays.[5]

In situ X-ray scattering studies provide detailed information on the formation and growth of inorganic nanomaterials.[6a,b,c] Powder X-ray diffraction (PXRD) probes the average crystal structure as well as the microstructure of the sample, whereas total X-ray scattering and atomic pair distribution function (PDF) analyses make it possible to investigate structures without long-range order, such as discrete clusters in solution and small nanoparticles. Thus total scattering is ideal for in situ studies of precrystalline processes occurring during hydrothermal synthesis. The number of applications of total X-ray and neutron scattering are rapidly increasing,[7a,b,c] but few have attempted to target the highly challenging experimental conditions of hydrothermal and supercritical synthesis.[8a,b] Here, total scattering is used to provide previously unobtainable structural information about the initial transformation of molecular precursor complexes into pristine nanoparticles. In addition, in situ PXRD is used to follow the nanocrystal structure, size, and size distributions.

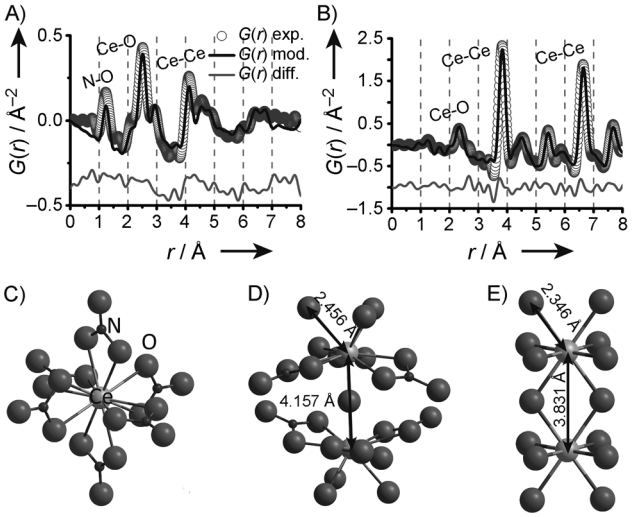

Figure 1. A) A PDF for the precursor solution and B) PDF for CeO_2 nanoparticles 60 seconds after initiation of the synthesis. Molecular complexes present in C) solid $(NH_4)_2Ce(NO_3)_6$ and D) the precursor liquid for CeO_2. E) Atomic arrangement in crystalline CeO_2 nanoparticles, 60 seconds after initiation of the synthesis.

The initial transformation from aqueous precursor medium to crystalline CeO_2 nanoparticles was investigated at 200 °C using in situ total X-ray scattering. Figure 1 A shows the pair distribution function (PDF) obtained for the dissolved $Ce(NH_4)_2(NO_3)_6$ precursor prior to heating. The cut-off distance of the PDF correlations is approximately 7 Å indicating the presence of local ordering only. In contrast, the low r region of the PDF obtained for well-ordered CeO_2 nanoparticles 60 seconds after initiation of the synthesis is

[*] C. Tyrsted, K. M. Ørnsbjerg Jensen, E. D. Bøjesen, Dr. N. Lock, Dr. M. Christensen, Prof. Dr. B. Brummerstedt Iversen
Center for Materials Crystallography
Department of Chemistry and iNANO, Aarhus University
Langelandsgade 140, 8000 Aarhus (Denmark)
E-mail: bo@chem.au.dk
Prof. Dr. S. J. L. Billinge
Applied Physics and Applied Mathematics
Columbia University, New York, NY 10027 (USA)
and
Condensed Matter Physics and Materials Science Department
Brookhaven National Laboratory, Upton, NY 11973 (USA)

[**] This work was supported by the Danish National Research Foundation (Center for Materials Crystallography), the Danish Strategic Research Council (Center for Energy Materials), the Danish Research Council for Nature and Universe (Danscatt), and the US National Science Foundation. The Advanced Photon Source is supported by the US Department of Energy, Office of Basic Energy Sciences.

Supporting information for this article is available on the WWW under http://dx.doi.org/10.1002/anie.201204747.

displayed in Figure 1B. A significant structural change occurs upon nucleation of CeO_2 as evidenced by the clear change in the shortest Ce-Ce distance (Figure 1A and B). The solid-state structure of the $Ce(NH_4)_2(NO_3)_6$ precursor is well-known and is comprised of monomeric Ce^{IV} ions octahedrally coordinated to six bidentate NO_3^- groups as shown in Figure 1C.[9] However, in solution it takes a different form: the PDF displayed in Figure 1A reveals that it exists as a structural intermediate between the dissolution of the crystalline precursor and the nucleation of crystalline CeO_2 nanoparticles. The observation of a sharp Ce-Ce peak at around 4.16 Å makes this conclusion unavoidable and suggests a dimer structure for the complex. The structure of this unknown precursor complex was found by fitting the PDF and is shown in Figure 1D. The calculated PDF from this molecular complex (black line, Figure 1A) is clearly visible in the PDF signal and well modeled despite being just about 7 Å in diameter and extracted from a large solvent signal. The molecular complex corresponds to two $Ce(NO_3)_6^{2-}$ octahedrons condensed to form a dimeric structure with the general formula $[(OH)_{6x}(NO_3)_{6(1-x)}CeOCe(NO_3)_{6(1-x)}(OH)_{6x}]^{6-}$, revealing a partial reaction between dissolved $Ce(NO_3)_6^{2-}$ complexes. The structure of the CeO_2 nanoparticles obtained 60 seconds after nucleation can be seen in Figure 1E for comparison.

The gradual shift of the shortest Ce-O and Ce-Ce interatomic distances of the precursor complex can be observed in Figure 2A together with the corresponding distances for CeO_2 at the time of nucleation. After 3 seconds the dimer complex coexists with pristine CeO_2 nanoparticles exhibiting a considerable difference in the Ce-O and Ce-Ce distances between the two phases. As the solvent reaches the set temperature within the first couple of seconds and nucleation commences, the dimer structure seems to contract, possibly because of weak dimer interactions. During the conversion of the dimer into ceria nanoparticles no continuous change in the bond distances is observed. Since the dimer is observed after the existence of nanoparticles, the assembly of dimers into larger clusters must be slow and rate-determining, because the concentration of these clusters is so low that it cannot be determined experimentally. To explain the pathway of this dimer assembly into ceria nanocrystals seems to to be interesting for future theoretical modeling. The gradual conversion of the precursor material into CeO_2 is quantified in Figure 2B which shows the evolution of the structural scale factors for the precursor and the CeO_2 nanoparticles based on the structural refinement of the time-resolved PDF.[10] At 200 °C the conversion of the precursor to the nanoparticles is completed after the first 10 seconds of the synthesis, and a slower evolution takes place over a much wider time-scale. The increase in the CeO_2 nanoparticle diameter after nucleation is shown in Figure 2C together with the time-resolved PDF in Figure 2D.

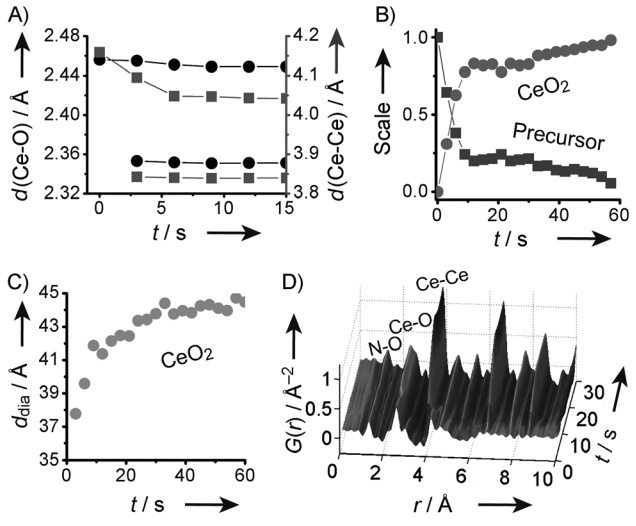

Figure 2. A) Evolution in the shortest interatomic Ce-O and Ce-Ce distances, d(Ce-O) and d(Ce-Ce), for the precursor complex and CeO_2. B) Normalized time-resolved evolution in the scale factor of the structural models for precursor and CeO_2 nanoparticles. C) Time-resolved evolution in the CeO_2 nanoparticle diameters (d_{dia}). D) Time-resolved evolution in the reduced pair distribution function.

To further study the growth of the nanocrystalline material after nucleation, in situ PXRD measurements were performed at a pressure of 230 bar and temperatures of 200, 300 (subcritical conditions), and 400 °C (supercritical water conditions, $T > 374$ °C, $P > 221$ bar). Figure 3A shows the evolution in the volume-averaged crystallite diameter of the CeO_2 nanoparticles, obtained from Rietveld refinement, and this diameter is shown to be heavily influenced by the synthesis temperature. Under supercritical conditions the crystallite size stabilizes at a diameter of about 16 nm, this diameter decreases to about9 nm at 300 °C and about 4 nm at 200 °C. Kinetic analysis of the growth curves was performed with a size-impediment model, $(D(t)^2 = D_{max}{}^2 - (D_{max}{}^2 - D_0{}^2)\exp[-k(t-t_0)])$.[11] The model parameters include the average grain size $D(t)$, with D_0 and D_{max} being the initial and equilibrium particle sizes, respectively. The growth rate is described by the k parameter, containing information about the specific interface energy and grain boundary mobility. The synthesis duration is described through time t and the onset time t_0. The growth rate can be converted to express the interfacial energy (γ) and grain boundary mobility (M) through $D_{max}{}^2 k/2 = 4\alpha\gamma M$, where α is a geometric constant.[11] The resulting equilibrium grain sizes and growth rates are $D(200\,°C) = 3.56(1)$ nm, $D(300\,°C) = 8.81(3)$ nm, $D(400\,°C) = 15.68(3)$ nm, $k(200\,°C) = 0.30(3)$ min^{-1}, $k(300\,°C) = 0.10(2)$ min^{-1}, and $k(400\,°C) = 0.65(2)$ min^{-1}. Using the approximations of constant interfacial energy (γ) and equal geometric constants (α) for spherical particles, the mobility is given as $M = D_{max}{}^2 k/8$ constant, or $M' = D_{max}{}^2 k/8$, giving $M'(200\,°C) = 0.5(1)$, $M'(300\,°C) = 1.0(2)$ and $M'(400\,°C) = 20.0(6)$. Thus, the in situ data suggest a highly nonlinear increase in the grain boundary mobility when the synthesis temperature is increased to supercritical conditions.

The in situ PXRD data were in addition analyzed by whole powder pattern modeling (WPPM).[12] Figure 3B shows the evolution in the crystallite size distributions, based on data recorded after 10 s, 20 s, 5 minutes, and 20 minutes. As expected the size distributions broaden and shift towards larger crystallite sizes with increased synthesis time. The samples synthesized at 200 °C retain a relative narrow size distribution relative to samples synthesized at

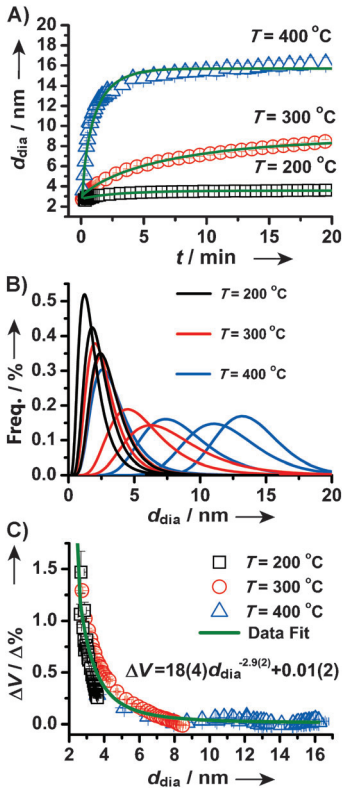

Figure 3. A) Volume-averaged crystallite diameters determined by Rietveld refinement of data obtained for the synthesis of CeO_2 nanoparticles at $T=200$, 300, and 400 °C. The calculated data points have been binned in a three-to-one ratio to emphasize the growth curves. B) Crystallite log-normal size distributions determined by WPPM of data obtained for the synthesis of CeO_2 nanoparticles synthesized at 200 °C (black line; 20 s, 1 minute, and 20 minutes), 300 °C (red line; 10 s, 20 s, 5 minutes, and 20 minutes), and 400 °C (blue line; 10 s, 20 s, 5 minutes, and 20 minutes). The frequency (Freq.) is defined as the percentage distribution at a given particle diameter. C) Change in the unit cell volume $[(V(D)-V_{min})/V_{min}\,100\,\%]$ presented as a function of volume-averaged crystallite diameter for CeO_2 synthesized at $T=200$, 300, and 400 °C (Δ% = volume expansion and d_{dia} = crystallite diameter).

400 °C, where the size distribution quickly broadens and reaches average sizes above 10 nm. The presence of a narrow crystallite size distribution at an early stage for $T=400$ °C corresponds well with an earlier study of small-angle X-ray scattering (SAXS) size distributions of CeO_2 synthesized in a continuous flow system at $T=375$ °C, with an effective heating duration of about 5 seconds.[13] In the case of TiO_2, it has been shown that increasing the temperature rather than the synthesis time is most effective for improving the crystallinity of the nanoparticles.[14] If this is transferred to the case of ceria, it is likely possible to synthesize very small but highly crystalline CeO_2 nanoparticles with narrow size distribution in less than 20 s under supercritical conditions.

Figure 3C shows the evolution in the nanoparticle unit cell dimensions based on Rietveld refinement of the PXRD data. In situ experiments are ideal for studies of size-dependent structural changes as they provide large numbers of directly correlated data, whereas ex situ data suffer from potential systematic differences between data points. The in situ data show a clear enlargement of the unit cell at low crystallite sizes (< 5 nm) whereas the unit cell dimensions are unchanged for sizes larger than 10 nm. Through modeling of the unit cell expansion (green curve in Figure 3C),[15] it is suggested that a unit cell volume expansion of 5% is achievable for 1.6(2) nm nanoparticles. The synthesis of nanoparticles with increased unit cell volumes is interesting as in the case of ceria-based oxygen conductors it has been speculated higher conductivities are achieved owing to a smaller migration enthalpy of the oxygen vacancies.[16a,b]

In situ total scattering studies of the hydrothermal synthesis of CeO_2 nanoparticles gives unprecedented insight into the structure of the precursor complexes, which transform into pristine CeO_2 nanoparticles. The total scattering data reveal that a 1 M aqueous solution of $(NH_4)_2Ce(NO_3)_6$ consists of dimeric Ce^{IV} nitrate complexes, which upon heating to 200 °C transform into CeO_2 nanoparticles in less than 10 seconds. In situ PXRD data show that highly crystalline 3–4 nm nanoparticles with narrow size distributions can be obtained in seconds for both hydrothermal and supercritical syntheses. The in situ data confirm a strong temperature dependence on the crystallite sizes which stabilize at about 4 nm at 200 °C, about 9 nm at 300 °C, and about 16 nm at 400 °C after 20 minutes of synthesis. The experimentally determined growth curves suggest a nonlinear increase in the grain boundary mobility when transcending from subcritical to supercritical synthesis conditions. A broadening in the nanoparticle size distributions is observed with increasing synthesis temperatures. The crystallographic unit cell was observed to be much increased for small nanoparticles with the bulk value being reached for particles > 10 nm. A maximum expansion of around 1.5% was seen for about 2.5 nm nanocrystals, and the data suggest expansions of up to 5% for particles below 2 nm. The present study provides direct evidence of the possibility to describe both atomic and microstructural changes during the hydrothermal synthesis of inorganic nanomaterials. The generality of the method renders these results a showcase from which important knowledge is obtainable for many different materials. The gained knowledge can in effect be used for the design of shape-tailored nanoparticles with specific properties.

Experimental Section

In situ measurements: A 1 M Ce^{4+} aqueous solution prepared from $(NH_4)_2Ce(NO_3)_6$ (Sigma Aldrich, > 98%) was used for the in situ syntheses in a custom-made capillary reactor pressurized to 230 bar and heated to temperatures of 200, 300, and 400 °C. The in situ total scattering PDF experiments were performed at beam line 11-ID-B at the Advanced Photon Source in the USA. In situ PXRD experiments were performed at beam line I711 at MAX-lab in Sweden. The experimental setup used for both the in situ total scattering and PXRD measurements has been described in detail by Becker et al.[5]

Data treatment: The integrated total scattering data were analyzed by the PDF method through the *PDFgetX3* program (unpublished results). Prior to the Fourier transform, the data were corrected for background scattering using measurements in deionized water in the same capillary at the appropriate temperatures. The resulting PDFs were refined sequentially in *PDFfit2* using *PDFgui*.[10] The structural refinement of CeO_2 is based on crystallographic data from ICSD-246969.[17] The structural refinement of the aqueous

precursor solution is based on crystallographic data on solid cerium oxide nitrate (ICSD-75163).[18]

Integrated PXRD data were modeled with the Rietveld method in *FullProf Suite*.[19] The instrumental contribution to peak-broadening was determined by refinement of a NIST LaB_6 pattern. The size broadening was described using a linear combination of cubic harmonics giving a Lorentzian description of the Bragg peak broadening.[20] The strain contribution to the Bragg peak broadening was taken into account by including a Gaussian profile parameter.

Whole powder pattern modeling (WPPM) was performed using the program PM2K.[21] The instrumental profile components were determined by a Cagliotti function fit to the LaB_6 diffraction pattern.[22] The size contributing part was implemented as originating from a log-normal size distribution of nanoscale scattering domains. Dislocation strain contributions were taken into account through a Wilkens model using the edge and screw dislocation contrast factors and Burgers vector modulus for a ceria crystal structure.[21]

Received: June 18, 2012
Published online: August 15, 2012

Keywords: crystal growth · hydrothermal synthesis · nanoparticles · X-ray diffraction · X-ray scattering

[1] A. Trovarelli, *Catal. Rev.* **1996**, *38*, 439 – 520.
[2] a) H. I. Chen, H. Y. Chang, *Ceram. Int.* **2005**, *31*, 795 – 802; b) A. Bumajdad, M. I. Zaki, J. Eastoe, L. Pasupulety, *Langmuir* **2004**, *20*, 11223 – 11233; c) T. Tsuzuki, P. G. McCormick, *J. Am. Ceram. Soc.* **2001**, *84*, 1453 – 1458; d) S. J. Shih, K. B. Borisenko, L. J. Liu, C. Y. Chen, *J. Nanopart. Res.* **2010**, *12*, 1553 – 1559.
[3] a) T. Adschiri, K. Kanazawa, K. Arai, *J. Am. Ceram. Soc.* **1992**, *75*, 1019 – 1022; b) P. Hald, J. Becker, M. Bremholm, J. S. Pedersen, J. Chevallier, S. B. Iversen, B. B. Iversen, *J. Solid State Chem.* **2006**, *179*, 2674 – 2680.
[4] V. H. Grassian, *J. Phys. Chem. C* **2008**, *112*, 18303 – 18313.
[5] J. Becker, M. Bremholm, C. Tyrsted, B. Pauw, K. M. O. Jensen, J. Eltzholt, M. Christensen, B. B. Iversen, *J. Appl. Crystallogr.* **2010**, *43*, 729 – 736.
[6] a) H. Jensen, M. Bremholm, R. P. Nielsen, K. D. Joensen, J. S. Pedersen, H. Birkedal, Y. S. Chen, J. Almer, E. G. Sogaard, S. B. Iversen, B. B. Iversen, *Angew. Chem.* **2007**, *119*, 1131 – 1134; *Angew. Chem. Int. Ed.* **2007**, *46*, 1113 – 1116; b) M. Bremholm, M. Felicissimo, B. B. Iversen, *Angew. Chem.* **2009**, *121*, 4882 – 4885; *Angew. Chem. Int. Ed.* **2009**, *48*, 4788 – 4791; c) N. Pienack, W. Bensch, *Angew. Chem.* **2011**, *123*, 2062 – 2083; *Angew. Chem. Int. Ed.* **2011**, *50*, 2014 – 2034.
[7] a) S. J. L. Billinge, M. G. Kanatzidis, *Chem. Commun.* **2004**, 749 – 760; b) P. J. Chupas, S. Chaudhuri, J. C. Hanson, X. Y. Qiu, P. L. Lee, S. D. Shastri, S. J. L. Billinge, C. P. Grey, *J. Am. Chem. Soc.* **2004**, *126*, 4756 – 4757; c) M. Estrella, L. Barrio, G. Zhou, X. Q. Wang, Q. Wang, W. Wen, J. C. Hanson, A. I. Frenkel, J. A. Rodriguez, *J. Phys. Chem. C* **2009**, *113*, 14411 – 14417.
[8] a) K. M. O. Jensen, M. Christensen, P. Juhas, C. Tyrsted, E. D. Boejesen, N. Lock, S. J. L. Billinge, B. B. Iversen, *J. Am. Chem. Soc.* **2012**, *134*, 6785 – 6792; b) C. Tyrsted, B. R. Pauw, K. M. O. Jensen, J. Becker, M. Christensen, B. B. Iversen, *Chem. Eur. J.* **2012**, *18*, 5759 – 5766.
[9] T. A. Beineke, J. Delgaudi, *Inorg. Chem.* **1968**, *7*, 715 – 721.
[10] C. L. Farrow, P. Juhas, J. W. Liu, D. Bryndin, E. S. Bozin, J. Bloch, T. Proffen, S. J. L. Billinge, *J. Phys. Condens. Matter* **2007**, *19*, 335219.
[11] H. Natter, M. Schmelzer, M. S. Loffler, C. E. Krill, A. Fitch, R. Hempelmann, *J. Phys. Chem. B* **2000**, *104*, 2467 – 2476.
[12] M. Leoni, T. Confente, P. Scardi, *Z. Kristallogr.* **2006**, *23*, 249 – 254.
[13] C. Tyrsted, J. Becker, P. Hald, M. Bremholm, J. S. Pedersen, J. Chevallier, Y. Cerenius, S. B. Iversen, B. B. Iversen, *Chem. Mater.* **2010**, *22*, 1814 – 1820.
[14] J. R. Eltzholtz, PhD thesis, Aarhus University (DK), **2012**.
[15] M. I. Ahmad, S. S. Bhattacharya, *Appl. Phys. Lett.* **2009**, *95*, 191906.
[16] a) F. Zhang, S. W. Chan, J. E. Spanier, E. Apak, Q. Jin, R. D. Robinson, I. P. Herman, *Appl. Phys. Lett.* **2002**, *80*, 127 – 129; b) B. C. H. Steele, *Solid State Ionics* **1984**, *12*, 391 – 406.
[17] S. Hull, S. T. Norberg, I. Ahmed, S. G. Eriksson, D. Marrocchelli, P. A. Madden, *J. Solid State Chem.* **2009**, *182*, 2815 – 2821.
[18] N. Guillou, J. P. Auffredic, D. Louer, *J. Solid State Chem.* **1994**, *112*, 45 – 52.
[19] J. Rodríguez-Carvajal, *Physica B* **1993**, *192*, 55 – 69.
[20] M. Järvinen, *J. Appl. Crystallogr.* **1993**, *26*, 525 – 531.
[21] M. Leoni, R. Di Maggio, S. Polizzi, P. Scardi, *J. Am. Ceram. Soc.* **2004**, *87*, 1133 – 1140.
[22] G. Caglioti, A. Paoletti, F. P. Ricci, *Nucl. Instrum. Methods* **1958**, *3*, 223 – 228.

